Research Article

Arginine dynamics probed by magic-angle spinning NMR with a specific isotope-labeling scheme

Darja I. Rohden [1,2,3,†], Federico Napoli [2,†], Anna Kapitonova [2], Ben P. Tatman [2], Roman J. Lichtenecker [1,4], and Paul Schanda [2,*]

*1 - **Faculty of Chemistry,** Institute of Organic Chemistry, University of Vienna, Währinger Str. 38, Vienna 1090, Austria*
*2 - **Institute of Science and Technology Austria,** Am Campus 1, Klosterneuburg 3400, Austria*
*3 - **Vienna Doctoral School in Chemistry (DoSChem),** University of Vienna, Währinger Str. 42, Vienna 1090, Austria*
*4 - **MAG-LAB,** Karl-Farkas Gasse 22, Vienna 1030, Austria*

***Correspondence to Paul Schanda:** paul.schanda@ist.ac.at (P. Schanda)*
https://doi.org/10.1016/j.jmb.2025.169379
Edited by Lewis E. Kay

Abstract

The specific introduction of ^{1}H-^{13}C or ^{1}H-^{15}N moieties into otherwise deuterated proteins holds great potential for high-resolution solution and magic-angle spinning (MAS) NMR studies of protein structure and dynamics. Arginine residues play key roles for example at active sites of enzymes. Taking advantage of a chemically synthesized Arg with a ^{13}C-$^{1}H_2$ group in an otherwise deuterated backbone, we demonstrate here the usefulness of proton-detected MAS NMR approaches to probe arginine dynamics. In experiments with crystalline ubiquitin and the 134 kDa tetrameric enzyme malate dehydrogenase we detected a wide range of motions, from sites that are rigid on time scales of at least tens of milliseconds to residues undergoing predominantly nanosecond motions. Spin-relaxation and dipolar-coupling measurements enabled quantitative determination of these dynamics. We observed microsecond dynamics of residue Arg54 in crystalline ubiquitin, whose backbone is known to sample different β-turn conformations on this time scale. The labeling scheme and experiments presented here expand the toolkit for high-resolution proton-detected MAS NMR.

Introduction

Nuclear Magnetic Resonance spectroscopy (NMR) is exquisitely suited to probe protein dynamics at a level of individual atoms. Its ability to sense amplitudes and time scales of motions, as well as its sensitivity to the local environment, and changes of the environment upon e.g. binding of a ligand or a conformational change, makes NMR a versatile method to address biophysical and biological questions. NMR can be applied to samples at ambient temperature in solution, as well as to "solid" states, including proteins embedded in membranes, large aggregates, sedimented proteins, crystals or entire cells/cell walls. A significant limitation for NMR is the size of the molecules that can be studied. On the one hand, in solution-state NMR, the slow overall tumbling of large molecules leads to rapid signal loss resulting in low sensitivity and broad lines. On the other hand, the number of atoms increases in large proteins, and so does the number of expected nuclear-spin signals; this leads to spectral congestion and signal overlap.

Technical developments have alleviated both challenges. In solution-NMR, the development of deuteration and methyl-labeling strategies (i.e. $^{13}C^{1}H_3$ labeling in an otherwise fully deuterated

environment) together with spin-relaxation optimized NMR pulse sequences have allowed to circumvent the aforementioned rapid signal loss. This methyl-transverse relaxation-optimized spectroscopy (TROSY) approach[1] allows solution-NMR studies of proteins ranging from hundreds of kilodalton to megadaltons in size.[2–5] For the case of methylene groups ($^{13}C^{1}H_2$), TROSY-based approaches are similarly capable of producing highest-resolution spectra, even of large proteins,[6] and add to amide-directed ^{1}H-^{15}N TROSY strategies.[7]

An alternative to eliminating line broadening caused by overall molecular tumbling is to suppress free Brownian motion entirely by using solid samples and applying rapid sample spinning at the magic angle (MAS NMR). In the absence of tumbling, linewidths in MAS NMR are independent of molecular size, enabling the study of large systems such as viral particles, cell walls, or protein assemblies, and providing access to structural and dynamic information at atomic resolution.

MAS NMR notoriously suffers from large linewidths, particularly in ^{1}H dimensions, which is due to the fact that MAS removes the effect of the strong dipolar couplings only incompletely, and in an MAS-frequency dependent manner. Although the advent of increasingly fast MAS also enables proton-detected studies of fully protonated proteins,[8–11] linewidths in protonated proteins remain significantly broader at presently achievable spinning rates compared to deuterated samples. Moreover, faster spinning comes at a substantial sensitivity cost. For example, a comparison between 1.3 mm rotors (spinning up to 60 kHz MAS) and 0.4 mm rotors (up to 160 kHz MAS) revealed more than a fivefold drop in absolute sensitivity,[9] translating to roughly 25-fold longer experiment times.

Deuteration (i.e. removing the large dipolar couplings to some ^{1}H spins) and the sparse incorporation of ^{1}H-^{13}C or ^{1}H-^{15}N spin pairs enables high-resolution ^{1}H-^{13}C and ^{1}H-^{15}N spectra.[12] Moreover, these more isolated spin systems are also useful when probing dynamics, because the spin evolution is much simpler, and artefacts that may hamper quantitative dynamics studies, such as dipolar dephasing, are largely suppressed. A number of specific isotope-labeling schemes have been used in MAS NMR recently. Methyl labeling, adopted from approaches originally introduced for solution-NMR,[13] has been used to determine protein structures[14–17] or to investigate side chain dynamics.[18–20] Labeling of aromatic side chains with single ^{1}H-^{13}C pairs allows probing aromatic ring flips and breathing motions of proteins.[21–23] The introduction of ^{1}H spins at the α-position,[24] the use of a complex mixture of isotope-labeled amino acids,[25] or the fractional/random sparse introduction of ^{1}H spins at aliphatic sites have also been proposed[26,27] and their relative merits have been discussed elsewhere.[11]

Arginine is an important residue at many active sites of enzymes, involved in protein-protein interactions and phase separation.[28] The positively charged terminal guanidino group is involved in charge-charge and cation-π interactions, crucial in the binding of negatively charged substrates such as carboxylic acids, nucleosides and DNA;[29] arginine modifications and cross-linking have been associated with regulation of cellular processes and tissue pathogenesis;[30,31] its structural and dynamical properties have been intensively studied.[32–34] With the goal of detecting arginine dynamics in large proteins, we have recently reported the chemical synthesis of arginine with a ^{13}C-$^{1}H_2$ moiety at the δ-position, a ^{15}N at the ε-position, and deuterated elsewhere (Arg-[$^{13}C^{\delta}$,$^{15}N^{\varepsilon}$,$^{2}H_4^{\beta,\gamma}$]; see Fig. 1A).[35] We showed that this amino acid is readily incorporated into proteins by bacterial expression and explored its use for protein-protein interactions.

In this study, we explore its use for MAS NMR, using crystalline ubiquitin as a model system and a large 134 kDa tetrameric enzyme, and compare the spectra with the solution-NMR spectra of the same proteins. Quantitative dynamics experiments (relaxation and dipolar-coupling measurements), which are sensitive to motions from nanoseconds to hundreds of microseconds, revealed differential dynamics of the different arginine side chains.

Results

MAS NMR spectra of arginines in ubiquitin point to differential dynamic behaviour

The 76-residue long ubiquitin comprises four arginine residues (R42, R54, R72, R74). Several previous MAS NMR studies of the structure and dynamics of ubiquitin have shown that the C-terminal residues are difficult to observe: the amide backbone sites of R72 to G76 in the MPD crystal form used here have remained invisible in both cross-polarization and *J*-coupling experiments.[36–38] Generally, CP-based transfers are efficient for rigid sites, whereas *J*-based transfers (INEPT) in solids allow seeing sites with large-amplitude motions.[39] It is known that there is a range of time scales (ca. $10^{6} - 10^{4}$ s^{-1}) in which signals are strongly attenuated in both types of experiments.[39] Detailed backbone dynamics studies of ubiquitin MPD crystals have been reported,[19,40–42] which revealed, *inter alia*, a μs conformational-exchange process in a β-turn that comprises residues 51–55 and 23–25.[41,43,44]

We produced deuterated ubiquitin labeled with arginine (Fig. 1A), referred to as u-[^{2}H,^{15}N],Arg-[$^{13}C^{\delta}$,$^{15}N^{\varepsilon}$,$^{2}H_4^{\beta,\gamma}$]) in a crystal form that has been

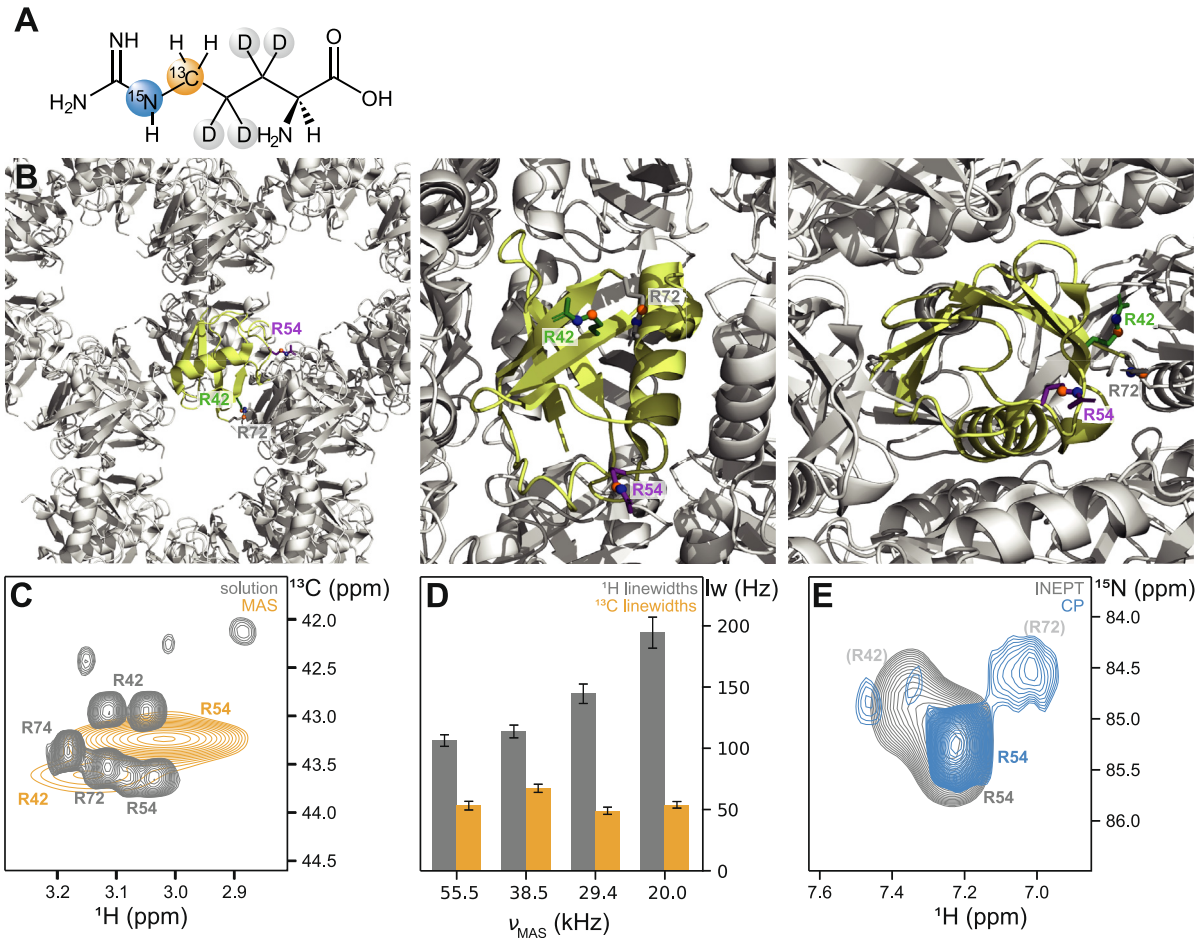

Fig. 1. Arginine labeling of ubiquitin crystals. (A) Molecular structure of the arginine isotopologue used in this study featuring a ^{13}C-$^{1}H_2$ moiety at the δ-position, and a ^{15}N at the ε-position.[35] (B) Structure of ubiquitin crystallized with MPD, corresponding to PDB entry 3ONS. R42, R54 and R72 are highlighted in green, purple and gray, respectively. R74 has not been modeled in the crystal structure. (C) ^{1}H-^{13}C HSQC spectrum of ubiquitin in solution (gray, 800 MHz) in comparison to a cross-polarization based hCH spectrum in the solid state (orange, 55 kHz MAS, 700 MHz). The signals of R42 and R54 were assigned using a 3D H^{δ}-(RFDR)-h^{N}-N–H^{N} experiment (see Fig. 2). (D) ^{1}H (gray) and ^{13}C (orange) homogeneous linewidths (*lw*) as a function of the MAS spinning frequency, determined by measuring the apparent coherence decay rate constant (R'_2) in a spin-echo experiment, reported as $lw = R'_2/\pi$. Details are provided in the Methods, and fit curves are shown in Fig. S1. (E) Comparison between a 2D NH spectrum recorded using an INEPT transfer (gray) and a CP transfer (blue) at 100 kHz MAS. The signal of R54 was assigned using a 3D H^{δ}-(RFDR)-h^{N}-N–H^{N} experiment (see Fig. 2C). R42 and R72 were assigned corresponding to BMRB entry 5387. (For interpretation of the references to colour in this figure legend, the reader is referred to the web version of this article.)

used in many MAS NMR[45] and crystallography studies,[46] using the precipitant methyl-pentanediol (MPD). We performed ^{1}H-detected correlation experiments at 55 kHz and 100 kHz MAS frequency directed to the arginine sites (Figs. 1C–E). In $^{13}C^{\delta}$-H^{δ} spectra one may expect four to eight signals from the four arginines: for a rigid Arg side chain the $^{1}H^{\delta 1}$ and $^{1}H^{\delta 2}$ sites are expected to give rise to distinct signals; in the presence of large-amplitude sub-ms motions, these would be averaged to one signal per Arg-δ site. The solution-NMR $^{1}H^{\delta}$-$^{13}C^{\delta}$ spectrum shows two signals for each R42 and R54 and a single, averaged signal for each R72 and R74 located in the highly flexible C-terminus. In the MAS NMR spectrum only two rather broad signals (in ^{1}H) are observed (Fig. 1C). We were able to assign these peaks to R42 and R54 using a 3D H^{δ}-(RFDR)-h^{N}-N–H^{N} experiment (see below). The larger linewidth precludes definite statements as to whether the corresponding peaks comprise two distinct signals, like in solution, or if they are averaged (further investigated below). Interestingly, the peak observed for R54 is 7.5 times more intense than that of R42, suggesting that the two sites undergo different dynamics.

Because the number of peaks is lower than the 4 to 8 expected signals, we speculated that very large-scale fast (ps-ns) dynamics may attenuate

the transfer of some of the sites in cross-polarization experiments. Thus, we recorded additional experiments with *J*-coupling based coherence transfer. Unlike CP-based approaches that rely on heteronuclear dipolar couplings (which are averaged by rapid isotropic motion), these experiments should achieve efficient polarization transfer for sites in fast exchange.[39] However, no additional peaks are observed (Fig. S2A). This observation points to short coherence lifetimes – fast transverse relaxation – of these signals, which are broadened beyond detection in both spectra. Moreover, the intensity of the INEPT-based spectrum is significantly lower (factor 10) than with cross-polarization. This is expected, as the refocused INEPT transfers are longer, i.e. 4 ms – 2 ms in the block converting H_x to $2H_yC_z$ and 2 ms in the block converting $2H_yC_z$ to C_y – against the 2.2 ms of CP. During this time, signals relax due to the strong anisotropic interactions.

To obtain a quantitative picture of the linewidths, we have measured coherence lifetimes (^{1}H and ^{13}C T_2') at different MAS frequencies (20–55.5 kHz; Fig. 1D and Fig. S1). ^{13}C coherence lifetimes do not significantly depend on the MAS frequency in this range and the homogeneous linewidth ($lw = R_2'/\pi$) is ca. 50 s^{-1} ($R_2 \approx 160$ s^{-1}). Homogeneous linewidths of ^{1}H decrease by almost a factor of two when the MAS rate is increased from 20 to 55.5 kHz. An MAS dependency is expected and is also found for e.g. amide ^{1}H spins in an otherwise deuterated protein.[11] It is interesting to compare the absolute number ($lw \approx 100$ Hz at 55 kHz) in this CH_2 moiety to those found for other moieties: in various protonated and deuterated samples, amide ^{1}H homogeneous linewidths (derived from R_2') at 55 kHz are of the order of 250 Hz (protonated) and 30–50 Hz (deuterated; see Fig. 13 in ref 11). The homogeneous aliphatic linewidths in protonated samples are on the order of 180 Hz (GB1)[10] to 400 Hz (Fig. S1 of reference 11). In deuterated and methyl-labeled proteins, ^{1}H lines are sharper, approximately 40 Hz (CHD_2) to 90 Hz (CH_3).[47,48] Line widths of the order of 40 Hz have also been reported for aromatic labeling.[22] Overall, the ^{1}H linewidths of the arginines in ubiquitin are clearly better than those of fully protonated samples, but somewhat broader than those of other specific ^{1}H-^{13}C labeled sites. We attribute this finding to the coupling within the CH_2 site and to the vicinal H^ε, as well as ns-μs motion, investigated further below.

Residue-specific assignments of Arg signals by through-space ^{1}H-^{1}H contacts

Ubiquitin's arginine $^1H^\delta$-$^{13}C^\delta$ and $^1H^\varepsilon$-$^{15}N^\varepsilon$ sites have previously not been assigned in crystalline samples (with the exception of the $^{13}C^\delta$ frequency of Arg 54[36,38]). To assign the observed signals, we resorted to experiments that connect side chain hydrogens to the (assigned) backbone amide moieties through the ^{1}H-^{1}H dipolar coupling. We reintroduced the dipolar coupling under MAS using a radiofrequency-driven recoupling (RFDR[49]) sequence, akin to the one previously used for assigning other side chain moieties.[22] Fig. 2A shows an overlay of the amide ^{1}H-^{15}N spectrum with H-N planes extracted at different ^{1}H positions of the H-H-N experiment. Although the $^1H^\delta$ frequencies of the two observed Arg-δ peaks partly overlap, we could clearly distinguish the cross-peaks, and identify eighteen cross-peaks to backbone amide sites, which allowed us to assign the two observed $^1H^\delta$-$^{13}C^\delta$ signals (see Fig. 2A-C). In a separate H-H-N experiment, centered on the $^{15}N^\varepsilon$ frequency, we detected a strong cross-peak from the $^1H^\varepsilon$-$^{15}N^\varepsilon$ peak to the $^1H^\delta$ frequency of R54, thus allowing to assign the strong $^1H^\varepsilon$-$^{15}N^\varepsilon$ peak to R54. There are two weaker signals in the $^1H^\varepsilon$-$^{15}N^\varepsilon$ spectrum (Fig. 1D), which do not feature cross-peaks in the RFDR experiment. We tentatively assign those to R42 and R72, based on the following considerations: The signal at 7.4 ppm/84.8 ppm has strongly diminished intensity in the INEPT-based experiment compared to the CP experiment, pointing to rapid coherence decay. Given that the assigned R42 $^{13}C^\delta$ spin has rapid transverse relaxation (see below, Fig. 3A,B), we assume that also the ε-site has rapid relaxation, and thus, assign this peak to R42. The signal at 7.0 ppm/84.5 ppm, which is visible only in INEPT but not in CP-based experiments, is tentatively assigned to R72.

Quantitative measurements of arginine dynamics

The fact that only two of the four arginines are visible and that they have substantially different intensities and different behaviour in INEPT and CP-based experiments points to a range of dynamic behaviors. In order to obtain a more precise view of the arginine dynamics, we measured ^{13}C and ^{15}N spin relaxation as well as ^{1}H-^{13}C and ^{1}H-^{15}N dipolar couplings. In MAS NMR, where overall tumbling is absent, spin-relaxation rate constants are sensitive to motions on a wide range of time scales[51–54] (see Fig. S5 for an overview of the expected spin relaxation for motions on different time scales). Dynamics on ns time scales lead to elevated longitudinal relaxation (R_1) rate constants, while motion on time scales of hundreds of ns to hundreds of μs induces rapid rotating-frame relaxation ($R_{1\rho}$). When measuring $R_{1\rho}$ over a range of spin-lock radiofrequency (RF) field strengths (ν_1), the dependency of $R_{1\rho}$ on ν_1 provides further insights into dynamics: in the low ν_1 regime, $R_{1\rho}$ increases with decreasing ν_1 if the site undergoes μs-ms motions that involve chemical-shift fluctuations (Bloch-McConnell relaxation dispersion, BMRD[55]); in the regime where ν_1 approaches the MAS frequency (ν_{MAS}), reorientations of the bond (dipolar coupling and CSA) on the μs-ms time scales lead to a rise of $R_{1\rho}$ as ν_1

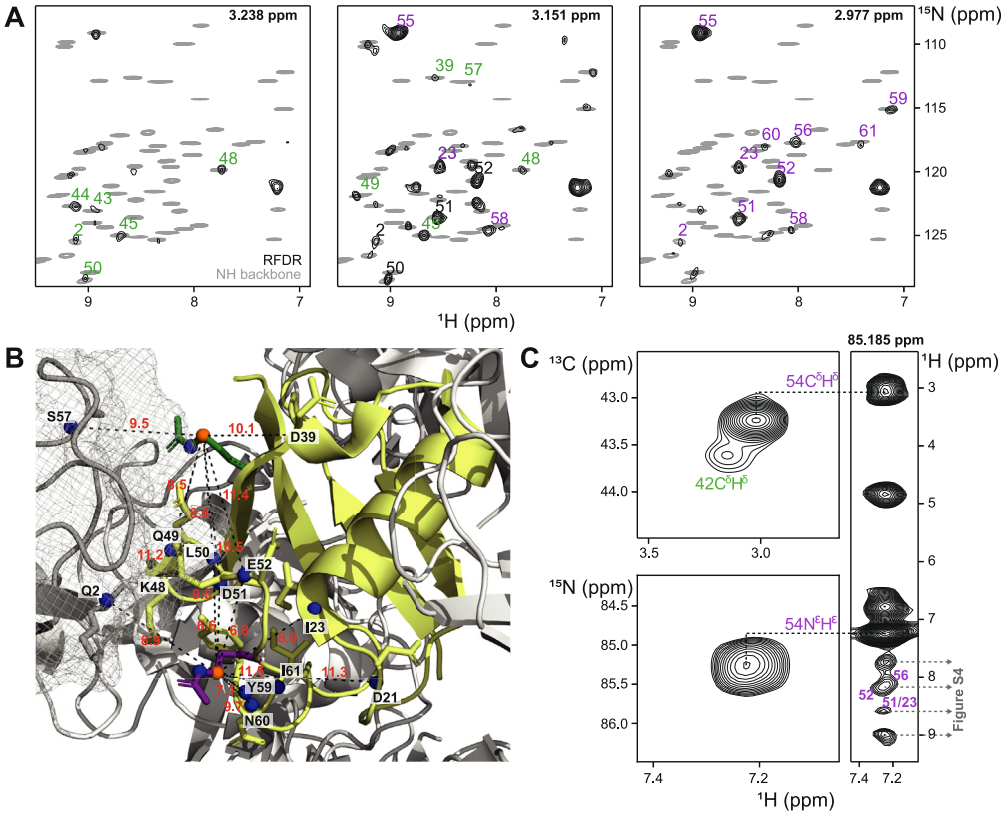

Fig. 2. Through-space connectivity from arginine C–H signals to backbone amide sites in ubiquitin. (A) Strips extracted from a 3D H^{δ}-(RFDR)-h^{N}-N–H^{N} experiment at three different H^{δ}-frequencies chosen to see the contacts between the $42C^{\delta}H^{\delta}$ (green) and $54C^{\delta}H^{\delta}$ (purple) signals and backbone amide sites. Contacts with both signals are labeled in black. For orientation, the NH backbone spectrum is shown in gray. (B) Structural representation of the contacts seen in the RFDR spectrum. R42 and R54 are shown in green and purple, respectively. Distances between the $C^{\delta}H^{\delta}$ and the amides are indicated in red. (C) ^{1}H-^{13}C (top left) and ^{1}H-^{15}N (bottom left) CP spectra showing the labeled arginine $C^{\delta}H^{\delta}$ and $N^{\varepsilon}H^{\varepsilon}$ sites. On the right, a strip from the 3D RFDR at the N^{ε} is shown, which was used to assign the signal to R54. The full amide ^{1}H-^{15}N spectrum is shown in Fig. S4. The ^{1}H frequencies indicated with dashed lines here are reported on the backbone spectrum there. (For interpretation of the references to colour in this figure legend, the reader is referred to the web version of this article.)

gets closer to ν_{MAS}. We termed the latter effect NEar-rotary Resonance Relaxation Dispersion (NERRD).[41] Conversely, a flat NERRD profile with elevated $R_{1\rho}$ rate constants points to motions on the hundreds of ns time scale.

Experimentally determined ^{13}C spin relaxation rate constants are shown in Fig. 3A-C. Of note, the $R_{1\rho}$ relaxation-dispersion profiles show rising rate constants at low (BMRD) and high (NERRD) RF field strengths. To translate these rate constants to dynamic parameters, we subjected the R_1 rate constants (one condition) and six $R_{1\rho}$ rate constants to a detectors analysis.[50] The detectors approach analyzes the amount of motion present in certain "time windows" (detectors), thereby taking into account the time scales to which the experimentally measured relaxation parameters are most sensitive. These detectors for our $^{13}C^{\delta}$ relaxation measurements are shown in Fig. 3D (left). The amplitudes of motions within each of these detectors are reported in the same panel (right). Most interestingly, there is a clear difference in the amount of motion in the slowest detector, i.e. on the time scale of tens of μs: R54 shows much more motion on this time scale than R42. This is in very good agreement with the observation that the backbone in this region (residues 51 to 55) undergoes motion on the μs time scale. We propose that the side chain of R54 senses this backbone dynamics. R42, however, which has even higher $R_{1\rho}$ rate constants than R54, exhibits motions on shorter time scales (ρ_1 detector).

We additionally measured dynamics through $^{15}N^{\varepsilon}$ spin relaxation ($R_1, R_{1\rho}$), using only the largest signal, corresponding to R54 at 100 kHz MAS. Recording NERRD data at this high MAS frequency would require ^{15}N RF fields approaching 100 kHz, which is not possible due to hardware limitations, and we focused on the Bloch-McConnell RD regime. The flat dispersion profile reveals that R54-$^{15}N^{\varepsilon}$ does not experience isotropic chemical-shift fluctuations on time scales of tens of μs to a

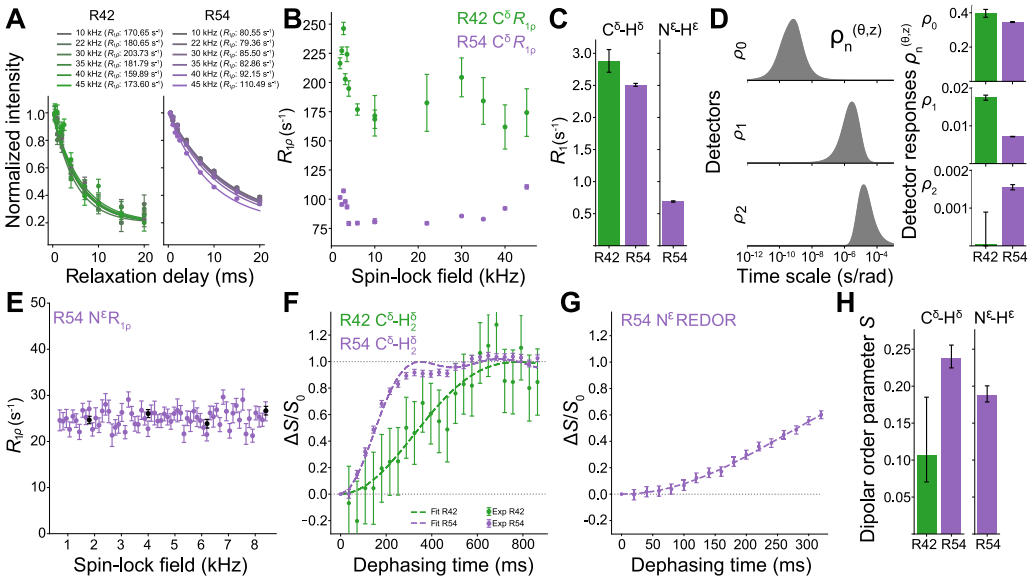

Fig. 3. Quantitative dynamics measurements of arginine side chains from relaxation and dipolar-coupling measurements. (A) $^{13}C^{\delta}$ $R_{1\rho}$ relaxation decays for arginines 42 and 54. (B) $^{13}C^{\delta}$ $R_{1\rho}$ relaxation dispersion profiles. (C) $^{13}C^{\delta}$ and $^{15}N^{\varepsilon}$ R_1 relaxation rates. Spectra underlying these fits are shown in Fig. S6. (D) Detectors[50] sensitivities (left) and responses (right), reporting on site-specific amplitudes of motion within the defined correlation time windows. (E) $^{15}N^{\varepsilon}$ $R_{1\rho}$ relaxation dispersion profiles in the BMRD regime. The black data points were obtained from a full time series (sampling 8 spin-lock durations up to 100 ms) while the purple points were obtained from a single time point (40 ms). (F) REDOR recoupling curves for dipolar-coupling measurements of the $C^{\delta}H^{\delta}_2$ and (G) of the $N^{\varepsilon}H^{\varepsilon}$ sites. (H) Fitted dipolar order parameters from the REDOR experiments.

few ms (Fig. 3E). This appears surprising, as the neighboring atom, C^{δ}, has a non-flat BMRD, and also undergoes dipolar-coupling fluctuations (NERRD) on the μs time scale. A possible explanation is that the N^{ε}, further out in the side chain, experiences a smaller chemical-shift fluctuation, possibly due to faster large-amplitude motions.

We probed the motional amplitude of the Arg side chains directly by measuring how dipolar couplings are averaged by motion. Dipolar-coupling tensors are averaged by motions faster than several tens of μs.[39] We measured ^{1}H-$^{13}C^{\delta}$ and ^{1}H-$^{15}N^{\varepsilon}$ dipolar-coupling strengths using Rotational Echo Double Resonance (REDOR) experiments (Fig. 3-F-H). The dipolar recoupling profiles show a clearly distinct behaviour of R42 and R54, with a twofold higher order parameter S of R54, although both have rather low values of S (below 0.25). The order parameter of the N^{ε} site is slightly lower than that of the C^{δ} site, which is expected due to its location further out in the side chain.

In summary, the specific Arg labeling allows the quantitative analysis of side chain dynamics over many time scales, including those that are very difficult to access by solution-state NMR. We have presented evidence that the Arg side chain of residue 54 senses a μs process that had so far only been reported for the backbone.

Application of the arginine labeling approach to a large enzyme complex with solution and MAS NMR

To explore the applicability of the arginine labeling approach for large proteins, we prepared the tetrameric 134 kDa large enzyme malate dehydrogenase (4 x 310 residues) from *Ignicoccus islandicus* (*I. islandicus*). Each monomer contains 20 arginines, the majority of which are involved in polar contacts in the available crystal structure (PDB ID: 6QSS).[56] Ten are localized on the protein surface, while five distribute at the dimer-dimer interface. Several highly conserved arginines are crucial in the malate/lactate dehydrogenases super-family, such as R86 and R154, which coordinate the two carboxyl ends of malate, and R92, which stabilizes the transition state during catalysis[57] (residue numbering referred to the *I. islandicus* sequence). For this reason, arginines are compelling targets for the study of this super-family.

Fig. 4 shows a CP-based 2D hCH experiment in orange. The spectrum contains numerous signals with dynamically averaged ^{1}H frequencies (at ca. 3 ppm and above) as well as pairs of signals that we ascribe to rigid side chains, i.e. with distinct signals for the two non-equivalent $^{1}H^{\delta}$ spins. Three of these exhibit more upfield chemical

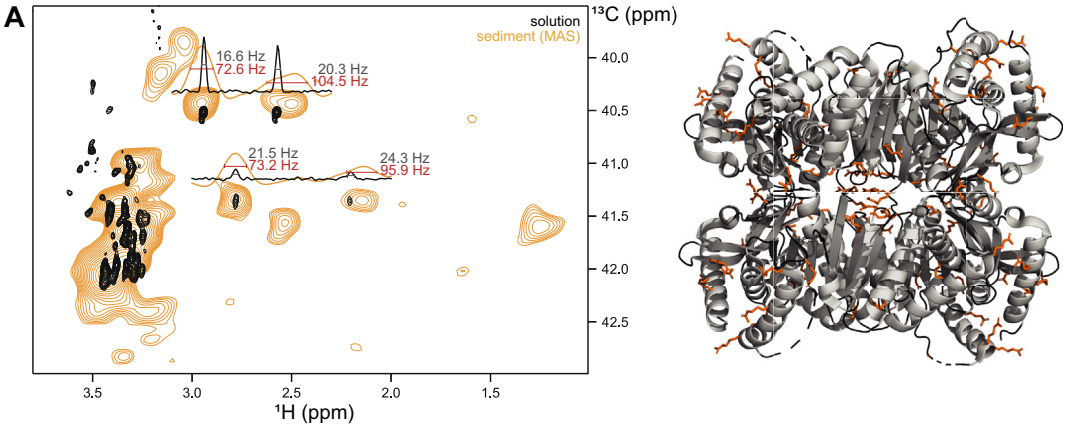

Fig. 4. Arginine labeling in a sedimented sample of the 4 × 33.5 kDa-large enzyme malate dehydrogenase from *I. islandicus*. (A) Arginine spectra in solution (black) and in a sedimented sample under MAS (orange). The solution-state experiment was performed at 800 MHz ^{1}H Larmor frequency using a TROSY-based experiment.[6] The MAS experiment, acquired at 700 MHz, was a CP-based hCH experiment. (B) Crystal structure of malate dehydrogenase from *I. islandicus* corresponding to PDB entry 6QSS. Arginines are highlighted in orange. (For interpretation of the references to colour in this figure legend, the reader is referred to the web version of this article.)

shifts, below 3 ppm, and can probably be ascribed to residues buried in hydrophobic cores, more shielded and constricted in their motion. Analogously, an analysis of assignment depositions from the BMRB database revealed a modest correlation between large chemical shift differences of the two non-equivalent $^{1}H^{\delta}$ spins and their upfield mean frequency (Fig. S3). In ubiquitin, no such pairs with strongly distinct $^{1}H^{\delta}$ frequency were observed. In an INEPT-based version of the same spectrum, the majority of the peaks are severely broadened, with the exception of the two at around 40 ppm, likely arising from highly flexible sites (Fig. S2B).

For comparison, we have recorded a solution-state NMR CH_2 TROSY spectrum. Overall, these spectra are in good agreement with each other in terms of peak positions, with some exceptions. Interestingly, in the solution-NMR spectrum a few extra peaks can be observed around 3.5 ppm. These could correspond to solvent-exposed sites, which experience less electronic shielding and are therefore shifted downfield. Surprisingly, the flexible sites, which survived the INEPT transfer in solids, cannot be observed in the solution state spectrum. Moreover, only two of the three upfield rigid pairs are visible. These observations may point to extensive broadening of this more rigid site because of the slow overall tumbling, and differences in dynamics of the side chains due to different sample temperatures (50 °C in solution, 30 °C in MAS NMR). The linewidths in the solid state are significantly larger than in solution, such that in the part of the spectrum where the dynamically averaged C^{δ}-H^{δ} moieties resonate, most of the signals are severely overlapped in the MAS NMR spectrum but less so in solution. The apparent ^{1}H linewidths of isolated peaks in the MAS NMR spectrum are in the range of 70 to 105 Hz (Fig. 4A), similarly to those of crystalline ubiquitin.

Overall, the application to the 134 kDa large malate dehydrogenase establishes that this labeling is suitable to probe dynamics and interactions also in large proteins. While the hyperthermophilic malate dehydrogenase used here can also be studied in solution at high temperature, it is noteworthy that at low temperatures or for even larger proteins, solution NMR may not be feasible or linewidths may exceed those of MAS NMR experiments.

Conclusions

We have explored here the labeling of arginine side chains with isolated $^{1}H^{\delta}_{2}$-$^{13}C^{\delta}$-$^{15}N^{\varepsilon}$ spin systems in an otherwise deuterated environment, in particular for proton-detected MAS NMR. As overall tumbling is absent in solids, a wide variety of MAS NMR methods allows probing dynamics on multiple time scales. We have illustrated this potential here with the measurement of various relaxation and relaxation-dispersion parameters as well as dipolar order parameters. For the case of ubiquitin's R54, we have demonstrated that the side chain senses μs motions, which is likely the same process that has been reported earlier for the backbone of this region of the protein.

Spectral resolution can be a challenge for this approach, in particular for the Arg sites that undergo fast dynamics and have (near) degenerated $^{1}H^{\delta}$ frequencies, as highlighted with the application to the 134 kDa large MalDH. However, for those arginines that are locked in one conformation, clearly distinct doublet signals are readily identified even in this large system. A possible future improvement may be the

stereospecific introduction of a single ^{1}H in the methylene group.

We foresee that site-specific labeling of a single Arg in the protein may bring this sensitive proton-detected MAS NMR/labeling approach to its full fruition. This approach, demonstrated for other amino-acid types,[58] would allow seeing Arg residues, e.g. in the active site of large enzymes, and probing their dynamics similarly as explored here.

Methods

Protein production

To produce human ubiquitin (UniProt accession number P0CG48), a pET-21a(+) vector was transformed into *E. coli* strain BL21(DE3) competent cells (Novagen) following standard protocols for the heat shock method. Cells were grown in M9 minimal medium in D_2O. For optimal cell growth, the D_2O content was increased stepwise (from 0 to 50 to 100%) in three precultures. The expression culture was supplemented with 1 g L^{-1} $^{15}NH_4Cl$ and 2 g L^{-1} glucose-$^{12}C^{2}H$ for uniform ^{15}N and ^{2}H labeling, respectively, and started at OD_{600} = 0.2. Isotopically labeled Arg-[$^{13}C^{\delta}$,$^{15}N^{\varepsilon}$,$^{2}H_4^{\beta,\gamma}$] (synthesized as reported recently[35]) was added at OD_{600} = 0.6 to a final concentration of 85 mg L^{-1}. Protein expression was induced 30 min after arginine addition using IPTG (1 mM). After 3.5 h, cells were harvested by centrifugation (2 × 15 min, 4,000 rcf). The cell pellets were resuspended in 50 mM Tris–HCl, pH 8.0 (buffer A) supplemented with protease inhibitor (cOmplete™, EDTA-free) and lysed by sonication with a Q700 ultrasonic processor (Qsonica) at 50% amplitude for a total operating time of 4 min. The lysate was subjected to a heat shock at 70 °C for 10 min. After centrifugation (40 min, 30,000 rcf, 4 °C), the buffer was exchanged to buffer A. The protein solution was purified by anion exchange chromatography (Cytiva, Resource™ Q) using a gradient from buffer A to B (50 mM Tris–HCl, 1 M NaCl, pH 8.0), and further by size exclusion chromatography (HiLoad 16/600 Superdex 75 PG column, Sigma–Aldrich) using buffer A as eluent. The protein solution was concentrated to 18.5 mg mL^{-1} using an Amicon 3.5 kDa concentrator (Millipore) and kept at −70 °C.

Ubiquitin crystals were obtained as described previously[45] using 2-methyl-2,4-pentanediol (MPD) as a crystallization agent: lyophilized ubiquitin was dissolved at a concentration of 20 mg mL^{-1} in buffer C (20 mM ammonium acetate, pH 4.2, H_2O based). Buffer D (50 mM citrate, pH 4.2) was mixed with MPD in a 40:60 volume ratio. A volume of 500 μL of this mixture was added to the bottom wells of 24-well sitting-drop crystallization plates (each with a 1.5 ml reservoir volume). The protein solution (37 μL) was then combined with 10 μL of the buffer D/MPD mixture and placed as a sitting drop in the wells of 24-well crystallization plates. The plates were sealed with adhesive tape and incubated at 4 °C. Sea-urchin like structures consisting of needle shaped crystals with a diameter of 10 μm and a length of 50 μm formed after 1–2 weeks.[46] These micro crystals were transferred into a 1.3 mm and a 0.7 mm rotor (Bruker), using in–house built ultracentrifuge devices (Beckman SW32 rotor, 20000 rpm, overnight). To prevent dehydration of the 1.3 mm rotor during measurement, a small drop of epoxy glue was applied between the rotor sleeve and the bottom cap prior to closing the cap; on the side of the drive cap, a FKM rubber spacer was inserted. The caps of the 0.7 mm rotor were not glued, and no spacers were inserted.

The wild-type sequence of *Ignicoccus islandicus* malate dehydrogenase (*Ii*MalDH) (UniProt accession number A0A0U3FQH7) was cloned into a pET-21a(+) plasmid. The protein was produced by bacterial over-expression in *E. coli* BL21(DE3) competent cells (Novagen). As for ubiquitin, M9 minimal medium in H_2O was used with a gradual adaptation to ^{2}H: first 50% D_2O, then D_2O was used. For uniform ^{15}N and ^{2}H labeling, the expression medium was supplemented with 1 g L^{-1} $^{15}NH_4Cl$ and 2 g L^{-1} glucose-$^{12}C^{2}H$. To increase arginine incorporation, 0.5 mM spermidine were added to the culture at OD_{600} = 0.3,[2] followed by the isotope-labeled arginine (60 mg L^{-1}) at OD_{600} = 0.6. Protein expression was induced 30 min after arginine addition using IPTG (1 mM). Cells were harvested by centrifugation after 5 h of expression, and pellets were resuspended in buffer E (50 mM Tris–HCl, 50 mM NaCl, pH 7.0) supplemented with 0.025 mg mL^{-1} RNase, 0.05 mg ml^{-1} DNase, 2 mM $MgCl_2$ and protease inhibitor (cOmplete™, EDTA-free). Lysis was performed by sonication, using a Q700 ultrasonic processor (Qsonica), at 40% amplitude for a total operating time of 4 min. Cell lysates were heated to 70 °C for 20 min and subsequently centrifuged (40,000 rcf, 30 min, 4 °C). The supernatant was filtered, and protein purification was conducted using a Resource™ Q column (Cytiva) equilibrated in buffer E, eluting the protein using a linear gradient of buffer F (50 mM Tris–HCl, 1 M NaCl, pH 7.5) over 10 column volumes. Fractions were analyzed by SDS–PAGE (12.5% polyacrylamide). The protein was identified by its monomeric molecular weight (33.55 kDa) and concentrated using an Amicon 10 kDa concentrator (Millipore). The concentrated solution was loaded onto a HiLoad 26/600 Superdex 200 PG column (Sigma–Aldrich) equilibrated with buffer E. MAS rotors (Bruker) were filled for NMR measurements by ultracentrifugation in a custom-built centrifugal funnel device (Beckman SW32 rotor, 20,000 rpm, overnight).

2 At the time of the protein expression, experiments towards the increase of incorporation rate by the addition of polyamines were conducted. The results indicated a slight improvement, but further studies are necessary. For details, see reference.[35]

NMR spectroscopy

All MAS NMR experiments were performed on a 700 MHz (16.45 T) Bruker NEO spectrometer using either a 1.3 mm probe with a coil tuned to ^{1}H, ^{13}C and ^{15}N frequencies and a supplementary ^{2}H coil (not used for this study), or a 0.7 mm ^{1}H, ^{13}C and ^{15}N probe (Bruker Biospin). Experiments performed with the 1.3 mm probe were conducted at a MAS frequency of 55.555 kHz (ca. 3.2 bar bearing pressure, 2.6 bar drive pressure). The cooling gas (1100 L h^{-1}, set-T 233 K) was set to reach an effective sample temperature of ca. 28 °C. Radio-frequency field strengths for hard pulses were ca. 108 kHz (^{1}H), 62 kHz (^{13}C) and 40 kHz (^{15}N) for experiments with the 1.3 mm probe.

The magic angle was adjusted directly on the protein sample at 55 kHz (1.3 mm) or 100 kHz (0.7 mm), respectively. We used the fact that in an INEPT H-N transfer, the interconversion of in-phase and anti-phase coherences proceeds with $\cos(\pi J + D_{res})t$ or $\sin(\pi J + D_{res})t$ where J is the known H-N scalar coupling and D_{res} is the dipolar coupling which is averaged by MAS, but has a non-zero value when the angle deviates from the magic angle $\arccos 1/\sqrt{2}$.[59] If the angle is correctly set, full transfer is expected when the delay is $1/(2J) \approx 5.4$ ms. We implemented a hNH experiment in which the H-N transfer is performed with a refocused INEPT and the N–H transfer with cross polarization, and set the phases such that the zero-crossing at 5.4 ms can be detected. Iterating the experiments with different angle settings allowed an accurate adjustment of the angle.

The measurement of ^{1}H-^{13}C dipolar couplings was performed at 55.555 kHz (τ_r=18 μs) using a shifted REDOR experiment[37,40] with cross-polarization steps for the H-C and C-H transfers. The REDOR pulses on the ^{1}H (^{13}C) channel were applied at a RF field strength of 100 kHz (62.5 kHz); the REDOR shift, applied to reduce the apparent oscillation frequency, was 3 μs, such that the shortest delay between consecutive ^{1}H pulse was 0.5 μs. The ^{1}H-^{15}N couplings were measured with a similar REDOR experiment, but with refocused INEPT transfers (H-N and N-H), at 100 kHz MAS frequency, and ^{1}H (^{13}C) pulses at 166.7 kHz (83.3 kHz) with a REDOR delay of 2 μs (i.e. a minimum delay between consecutive ^{1}H pulses of 0.5 μs).

Relaxation rate constants (bulk R_2', R_1 or $R_{1\rho}$) were determined by measuring intensity decays as a function of the relaxation delay (except for the one-point measurements, see below). For ^{13}C and ^{15}N R_1 measurements, delays of 0.005, 0.1, 0.2, 0.3, 0.4, 0.6, 0.8, 1 and 0.1, 0.5, 0.9, 1.2, 1.5, 1.8, 2.2, 3, 4 s were used, respectively. For $R_{1\rho}$ measurements, 8 delays up to 20 or 100 ms were used for ^{13}C and ^{15}N, respectively. For the ^{13}C $R_{1\rho}$ experiments, a single ^{1}H 180° pulse was applied in the center of the relaxation delay. We note that work in our group suggests that a continuous-wave ^{1}H decoupling should be applied, as some artefactual increases in $R_{1\rho}$ may otherwise occur.[60] The rise of $R_{1\rho}$ at low RF field strengths may partly be explained by this effect. The Bloch-McConnell part of the ^{13}C dispersions is shown in this work but not quantitatively exploited. In the ^{15}N, a 8 kHz ^{1}H CW decoupling was applied.

Bulk R_2' relaxation delays are reported in Supplementary Fig. S1. In the ^{1}H R_2' measurements, a hCH pulse sequence was modified to include a τ-^{1}H π-pulse-τ element after the initial ^{1}H excitation, without any decoupling during this delay. For the ^{13}C R_2' measurements, the τ-^{13}C π-pulse-τ element was inserted after the initial H-C CP, and ^{1}H swfTPPM decoupling was applied at an RF field strength of ca. 10 kHz (55.5 and 38.5 kHz MAS), 115 kHz (29.4 kHz MAS) and 100 kHz (20 kHz MAS).

The single-point measurements of $R_{1\rho}$ for Bloch-McConnell relaxation dispersion analysis were performed by measuring the peak intensity after irradiation for 40 ms as a function of the spin-lock RF amplitude, where this amplitude was varied from 0.7 to 8.4 kHz in 64 steps.

Solution-state NMR experiments were performed on a 800 MHz spectrometer equipped with a Bruker TCI cryo-probe. The sample temperature for measurements of ubiquitin was 25 °C, while the *Il*MalDH sample was measured at 50 °C. (Note that this differs from the MAS NMR experiment, which likely is responsible for some of the spectral changes.)

Data analysis

Intensities were extracted by fitting gaussian peaks using the Python package nmrglue.[61] For bulk R_2', the arginine $^{1}H^{\delta}$ regions of 1D spectra were integrated. Errors on the intensities were obtained by computing the standard deviation of signal in empty regions of the 1D/2D spectra. To obtain relaxation rates, intensities were fitted to a mono-exponential decay using SciPy,[62] and plotted with Matplotlib.[63] Error estimates were determined through a Monte Carlo approach as described e.g. in ref. [64].

For the single-point measurements, intensities were extracted as above. Assuming that the anisotropic contribution to relaxation varies negligibly across these frequencies (a reasonable assumption, given the NERRD profiles recorded), we extracted offset $R_{1\rho}$ from these as:

$$R'_{1\rho}(\nu_1) + \text{offset} = -\frac{1}{40\text{ms}} \log(I(\nu_1)). \quad (1)$$

The offset component was determined by comparison with the full-time series measurements (see above), following which the $R'_{1\rho}$ and ν_1 were corrected for transmitter offset effects as $R_{1\rho} = \frac{R'_{1\rho} - \cos\theta R_1}{\sin\theta}$ and $\nu_{eff} = \sqrt{\nu_1'^2 + \Omega^2}$,

respectively, where $\theta = \arctan\frac{\nu_1}{\Omega}$, and Ω is the transmitter offset from the resonance of interest.

Relaxation rates were analyzed using the Detectors approach as implemented in the package Detectorist.[65] We included only $R_{1\rho}$ measurements with $\nu_1 \geqslant 10$ kHz, as below this the Bloch-McConnell Relaxation Dispersion component would become significant. Sensitivities were calculated assuming two heteronuclear ^{13}C-^{1}H dipolar couplings at a distance of 1.09 Å. Each sensitivity was quantized using 200 time points, logarithmically spaced between 100 fs and 1 ms.

Detector optimization was performed using the Singular Value Decomposition method.[66] A matrix, $\boldsymbol{M}$, was created in which each of the N rows represents the sensitivity of the corresponding relaxation rate. The singular value decomposition of this matrix was taken:

$$\boldsymbol{M} = \boldsymbol{U}\boldsymbol{\Sigma}\boldsymbol{V}'. \quad (2)$$

The $\boldsymbol{U}$ and $\boldsymbol{V}'$ matrices were truncated according to the k largest singular values (where k was varied from 2 to 7 for model selection). Linear programming was performed using SciPy[62] to optimize linear combinations of the orthogonal singular vectors in the truncated $\boldsymbol{V}'_k$ to identify well-formed detectors. The coefficients corresponding to each of the k singular vectors then form the rows of the transformation matrix $\boldsymbol{Q}$, which can be used to determine the matrix $\boldsymbol{r}$, containing 'detector vectors':

$$\boldsymbol{r} = \boldsymbol{U}_k\boldsymbol{\Sigma}_k\boldsymbol{Q}^{-1}, \quad (3)$$

for which each of the N columns, $\boldsymbol{r}_i$, gives a linear combination of $\leqslant k$ detectors giving the corresponding relaxation rate. The detector responses may then be determined using a Non-Negative Least Squares algorithm to solve for the detector responses, $\boldsymbol{\rho}$:

$$\boldsymbol{\rho} = \begin{bmatrix} \boldsymbol{r}_1/e_1 \\ \vdots \\ \boldsymbol{r}_N/e_N \end{bmatrix}^{-1} \frac{\boldsymbol{R}}{\boldsymbol{e}}, \quad (4)$$

where $\boldsymbol{R}$ and $\boldsymbol{e}$ are vectors containing the experimental relaxation rates and uncertainties, respectively. The detector sensitivities are obtainable directly from the product $\boldsymbol{Q}\boldsymbol{V}'_k$. The number of singular values to be included in the analysis was identified by performing the analysis for $k = 2$ to 7, back-calculating the relaxation rates, and determining the reduced χ^2 and corrected Akaike Information Criterion (AICc). On the basis of this, we selected to include $k = 3$ detectors, as this gave the lowest reduced χ^2 and AICc for R42.

The REDOR data were analyzed to extract the dipolar-coupling anisotropy, using a grid-search procedure, akin to previous studies.[40] In brief, the intensities in the recoupled and reference experiments were used to calculate $\Delta S/S_0 = (S - S_0/S_0)$ (where S (S_0) are the peak intensities in the experiments without (with) recoupling pulses on the ^{1}H channels). As the intensity in the reference experiment hardly varies over the short time used for recoupling (< 1 ms), only 3 (NH) or 4 (CH) points were measured for the reference experiment and fitted to a straight line, which was used to interpolate S_0 for all time points. The dipolar-coupling anisotropy was obtained from the site-specific $\Delta S/S_0$ profiles by comparing the experimental data to a grid of numerically simulated REDOR curves (with incremented dipolar-coupling strength). For each simulated REDOR curve, the deviation from the experimental profile was calculated as a sum over all time points i of $\chi^2 = \sum_i((\Delta S/S_0)_i^{exp} - (\Delta S/S_0)_i^{sim})^2/\sigma_i^2$; a reduced chi-square χ^2_{red} was calculated by dividing χ^2 by the number of degrees of freedom, i.e. the number of REDOR points measured minus the number of fit parameters (which is one). The reported best-fit dipolar coupling strength is the one with the lowest χ^2_{red}. The reported uncertainties reflect the values of the dipolar coupling anisotropy over this array of simulated curves where the value of χ^2_{red} exceeds its minimum value by one. The numerical simulations were performed with the GAMMA package,[67] using explicit finite pulses according to the experimentally used timing. The ^{13}C CSA parameters for the δ-carbon were set to −45 ppm with an asymmetry of 0.9;[68] note that the CSA parameters have virtually no effect on REDOR curves.[69] The simulated spin system for the analysis of C^{δ} comprised two ^{1}H spins (separated by 1.8 Å and the ^{13}C spin (separated from each ^{1}H by 1.1 Å). The simulations for the analysis of the N^{ε} site comprised the N^{ε}, the H^{ε} spin, and the two adjacent H^{δ} spins. We also estimated the dipolar couplings of the backbone NH sites to ensure they are in a reasonable range compared to previous studies;[40] for these, only the amide N and H spins were considered. All analysis routines and GAMMA codes are available in the deposited data repository (see data availability section).

Author contributions

D. I. R. produced samples, analyzed data and produced figures. F. N. wrote analysis scripts and analyzed MAS NMR data. A. K. produced protein samples. B. P. T. performed the detectors analysis. R. L. supervised the synthesis part and contributed to the design of the labeling. P. S. recorded NMR experiments, analyzed the REDOR data and wrote the manuscript with input from all co-authors.

Data availability

Raw data, analysis scripts and figures have been deposited on the ISTA Research EXplorer (https://research-explorer.ista.ac.at/) with digital object identifier (DOI): 10.15479/AT-ISTA-19956.

DECLARATION OF COMPETING INTEREST

The authors declare the following financial interests/personal relationships which may be considered as potential competing interests: Roman Lichtenecker is shareholder in the company Mag-Lab. All other authors declare that they do not have competing interests.

Acknowledgements

This work was supported financially by the Austrian Science Fund (FWF, Grant No. I5812-B, “AlloSpace”). This research was supported by the Scientific Service Units (SSU) of Institute of Science and Technology Austria (ISTA) through resources provided by the Nuclear Magnetic Resonance Facility and the Lab Support Facility (LSF). We thank Petra Rovò and Margarita Valhondo Falcón for excellent support of the NMR facility.

Appendix A. Supplementary data

Supplementary data associated with this article can be found, in the online version, at https://doi.org/10.1016/j.jmb.2025.169379.

Received 3 July 2025;
Accepted 4 August 2025;
Available online 12 August 2025

Keywords:
protein dynamics;
deuteration;
specific isotope labeling;
solid-state NMR;
ubiquitin;
malate dehydrogenase

† Authors contributed equally

References

1. Ollerenshaw, J.E., Tugarinov, V., Kay, L.E., (2003). Methyl TROSY: explanation and experimental verification. *Magn. Reson. Chem.* **41** (10), 843–852.
2. Toyama, Y., Kay, L.E., (2021). Probing allosteric interactions in homo-oligomeric molecular machines using solution NMR spectroscopy. *Proc. Natl. Acad. Sci. USA* **118** (50), 1–12.
3. Mas, G., Guan, J.-Y., Crublet, E., Debled, E.C., Moriscot, C., Gans, P., Schoehn, G., Macek, P., Schanda, P., Boisbouvier, J., (2018). Structural investigation of a chaperonin in action reveals how nucleotide binding regulates the functional cycle. *Sci. Adv.* **4** (9), eaau4196.
4. Religa, T.L., Sprangers, R., Kay, L.E., (2010). Dynamic regulation of archaeal proteasome gate opening as studied by TROSY NMR. *Science* **328** (5974), 98–102.
5. Sprangers, R., Velyvis, A., Kay, L.E., (2007). Solution NMR of supramolecular complexes: providing new insights into function. *Nat. Methods* **4** (9), 697–703.
6. Miclet, E., Williams, D.C., Clore, G.M., Bryce, D.L., Boisbouvier, J., Bax, A., (2004). Relaxation-optimized NMR spectroscopy of methylene groups in proteins and nucleic acids. *J. Am. Chem. Soc.* **126** (34), 10560–10570.
7. Pervushin, K., Riek, R., Wider, G., Wüthrich, K., (1997). Attenuated T2 relaxation by mutual cancellation of dipole-dipole coupling and chemical shift anisotropy indicates an avenue to NMR structures of very large biological macromolecules in solution. *Proc. Natl. Acad. Sci. USA* **94** (23), 12366–12371.
8. Callon, M., Luder, D., Malär, A.A., Wiegand, T., Rímal, V., Lecoq, L., Böckmann, A., Samoson, A., Meier, B.H., (2023). High and fast: NMR protein–proton side-chain assignments at 160 kHz and 1.2 GHz. *Chem. Sci.* **14** (39), 10824–10834.
9. Z. Sun, C. Ollier, A. Rancz, B. Thienpont, K. Grohe, L. Becker, A. Purea, F. Engelke, S. Wegner, J. Sturgis, et al., Pushing the boundaries of resolution in solid-state nuclear magnetic resonance of biomolecules with 160 khz magic-angle spinning, J. Am. Chem. Soc.
10. Andreas, L.B., Jaudzems, K., Stanek, J., Lalli, D., Bertarello, A., Le Marchand, T., Cala-De Paepe, D., Kotelovica, S., Akopjana, I., Knott, B., Wegner, S., Engelke, F., Lesage, A., Emsley, L., Tars, K., Herrmann, T., Pintacuda, G., (2016). Structure of fully protonated proteins by proton-detected magic-angle spinning NMR. *Proc. Natl. Acad. Sci. USA* **113** (33), 9187–9192.
11. Marchand, T.L., Schubeis, T., Bonaccorsi, M., Paluch, P., Lalli, D., Pell, A.J., Andreas, L.B., Jaudzems, K., Stanek, J., Pintacuda, G., (2022). ^{1}H-detected biomolecular NMR under fast magic-angle spinning. *Chem. Rev.* **122** (10), 9943–10018.
12. Reif, B., (2022). Deuteration for high-resolution detection of protons in protein magic angle spinning (MAS) solid-state NMR. *Chem. Rev.* **122** (10), 10019–10035.
13. Goto, N.K., Gardner, K.H., Mueller, G.A., Willis, R.C., Kay, L.E., (1999). A robust and cost-effective method for the production of Val, Leu, Ile (delta 1) methyl-protonated ^{15}N-, ^{13}C-, ^{2}H-labeled proteins. *J. Biomol. NMR* **13** (4), 369–374.
14. Gauto, D.F., Estrozi, L.F., Schwieters, C.D., Effantin, G., Macek, P., Sounier, R., Sivertsen, A.C., Schmidt, E., Kerfah, R., Mas, G., Colletier, J.-P., Güntert, P., Favier, A., Schoehn, G., Schanda, P., Boisbouvier, J., (2019). Integrated NMR and cryo-EM atomic-resolution structure determination of a half-megadalton enzyme complex. *Nat. Commun.* **10** (1), 2697.
15. Huber, M., Hiller, S., Schanda, P., Ernst, M., Böckmann, A., Verel, R., Meier, B.H., (2011). A proton-detected 4D solid-state NMR experiment for protein structure determination. *ChemPhysChem* **12** (5), 915–918.
16. Linser, R., Bardiaux, B., Higman, V., Fink, U., Reif, B., (2011). Structure calculation from unambiguous long-range amide and methyl ^{1}H-^{1}H distance restraints for a microcrystalline protein with MAS solid-state NMR spectroscopy. *J. Am. Chem. Soc.* **133** (15), 5905–5912.
17. Zinke, M., Fricke, P., Lange, S., Zinn-Justin, S., Lange, A., (2018). Protein- protein interfaces probed by methyl labeling and proton-detected solid-state nmr spectroscopy. *ChemPhysChem* **19** (19), 2457–2460.
18. Xue, K., Mamone, S., Koch, B., Sarkar, R., Reif, B., (2019). Determination of methyl order parameters using solid state

NMR under off magic angle spinning. *J. Biomol. NMR* **73** (8), 471–475.
19. Schanda, P., Huber, M., Boisbouvier, J., Meier, B.H., Ernst, M., (2011). Solid-state NMR measurements of asymmetric dipolar couplings provide insight into protein side-chain motion. *Angew. Chem. Int. Ed.* **50** (46), 11005–11009.
20. Agarwal, V., Xue, Y., Reif, B., Skrynnikov, N.R., (2008). Protein side-chain dynamics as observed by solution- and solid-state NMR spectroscopy: a similarity revealed. *J. Am. Chem. Soc.* **130** (49), 16611–16621.
21. Becker, L.M., Berbon, M., Vallet, A., Grelard, A., Morvan, E., Bardiaux, B., Lichtenecker, R., Ernst, M., Loquet, A., Schanda, P., (2023). The rigid core and flexible surface of amyloid fibrils probed by magic-angle-spinning NMR spectroscopy of aromatic residues. *Angew. Chem. Int. Ed.* **62** (19) e202219314.
22. Gauto, D.F., Macek, P., Barducci, A., Fraga, H., Hessel, A., Terauchi, T., Gajan, D., Miyanoiri, Y., Boisbouvier, J., Lichtenecker, R., et al., (2019). Aromatic ring dynamics, thermal activation, and transient conformations of a 468 kDa enzyme by specific 1H–13C labeling and fast magic-angle spinning NMR. *J. Am. Chem. Soc.* **141** (28), 11183–11195.
23. Gauto, D.F., Lebedenko, O.O., Becker, L.M., Ayala, I., Lichtenecker, R., Skrynnikov, N.R., Schanda, P., (2023). Aromatic ring flips in differently packed ubiquitin protein crystals from MAS NMR and MD. *J. Struct. Biol. X* **7**, 100079.
24. Movellan, K.T., Najbauer, E.E., Pratihar, S., Salvi, M., Giller, K., Becker, S., Andreas, L.B., (2019). Alpha protons as NMR probes in deuterated proteins. *J. Biomol. NMR* **73**, 81–91.
25. Wang, S., Parthasarathy, S., Nishiyama, Y., Endo, Y., Nemoto, T., Yamauchi, K., Asakura, T., Takeda, M., Terauchi, T., Kainosho, M., et al., (2015). Nano-mole scale side-chain signal assignment by 1H-detected protein solid-state NMR by ultra-fast magic-angle spinning and stereo-array isotope labeling. *PLoS one* **10** (4), e0122714.
26. Medeiros-Silva, J., Mance, D., Daniëls, M., Jekhmane, S., Houben, K., Baldus, M., Weingarth, M., (2016). 1H-detected solid-state NMR studies of water-inaccessible proteins in vitro and in situ. *Angew. Chem. Int. Ed.* **55** (43), 13606–13610.
27. Asami, S., Schmieder, P., Reif, B., (2010). High resolution ^{1}H-detected solid-state NMR spectroscopy of protein aliphatic resonances: access to tertiary structure information. *J. Am. Chem. Soc.* **132** (43), 15133–15135.
28. Gupta, M.N., Uversky, V.N., (2024). Biological importance of arginine: a comprehensive review of the roles in structure, disorder, and functionality of peptides and proteins. *Int. J. Biol. Macromol.* **257**, 128646.
29. Zeymer, C., Fischer, S., Reinstein, J., (2014). trans-acting arginine residues in the AAA+ chaperone ClpB allosterically regulate the activity through inter- and intradomain communication. *J. Biol. Chem.* **289** (47), 32965–32976.
30. Mukherjee, J., Majumder, A.B., Gupta, M.N., (2016). Adding an appropriate amino acid during crosslinking results in more stable crosslinked enzyme aggregates. *Anal. Biochem.* **507**, 27–32.
31. Tsikas, D., (2021). Post-translaitonal modifications (ptm): analytical approaches, signaling, physiology and pathopysiology - part i. *Amino Acids* **53** (4), 485–487.
32. Gerecht, K., Figueiredo, A.M., Hansen, D.F., (2017). Determining rotational dynamics of the guanidino group of arginine side chains in proteins by carbon-detected NMR. *Chem. Commun.* **53** (72), 10062–10065.
33. Crowley, P.B., Golovin, A., (2005). Cation–π interactions in protein–protein interfaces. *Proteins: Struct., Funct., Bioinf.* **59** (2), 231–239.
34. Colletier, J.P., Aleksandrov, A., Coquelle, N., Mraihi, S., Mendoza-Barberá, E., Field, M., Madern, D., (2012). Sampling the conformational energy landscape of a hyperthermophilic protein by engineering key substitutions. *Mol. Biol. Evol.* **29** (6), 1683–1694.
35. Rohden, D.I., Toscano, G., Schanda, P., Lichtenecker, R. J., (2025). Synthesis of selectively ^{13}C/^{2}H/^{15}N-labeled arginine to probe protein conformation and interaction by NMR spectroscopy. *Chem. Eur. J.* **31** (24) e202500408.
36. Schubert, M., Manolikas, T., Rogowski, M., Meier, B.H., (2006). Solid-state NMR spectroscopy of 10% 13C labeled ubiquitin: spectral simplification and stereospecific assignment of isopropyl groups. *J. Biomol. NMR* **35** (3), 167–173.
37. Schanda, P., Meier, B.H., Ernst, M., (2010). Quantitative analysis of protein backbone dynamics in microcrystalline ubiquitin by solid-state NMR spectroscopy. *J. Am. Chem. Soc.* **132** (45), 15957–15967.
38. Fasshuber, H.K., Lakomek, N.-A., Habenstein, B., Loquet, A., Shi, C., Giller, K., Wolff, S., Becker, S., Lange, A., (2015). Structural heterogeneity in microcrystalline ubiquitin studied by solid-state NMR. *Prot. Sci.* **24** (5), 592–598.
39. Aebischer, K., Ernst, M., (2024). INEPT and CP transfer efficiencies of dynamic systems in MAS solid-state NMR. *J. Magn. Reson.* **359**, 107617.
40. Haller, J.D., Schanda, P., (2013). Amplitudes and time scales of picosecond-to-microsecond motion in proteins studied by solid-state NMR: a critical evaluation of experimental approaches and application to crystalline ubiquitin. *J. Biomol. NMR* **57** (3), 263–280.
41. Kurauskas, V., Izmailov, S.A., Rogacheva, O.N., Hessel, A., Ayala, I., Woodhouse, J., Shilova, A., Xue, Y., Yuwen, T., Coquelle, N., Colletier, J.-P., Skrynnikov, N.R., Schanda, P., (2017). Slow conformational exchange and overall rocking motion in ubiquitin protein crystals. *Nat. Commun.* **8**, 145.
42. Lorieau, J.L., McDermott, A.E., (2006). Conformational flexibility of a microcrystalline globular protein: order parameters by solid-state NMR spectroscopy. *J. Am. Chem. Soc.* **128** (35), 11505–11512.
43. Marion, D., Gauto, D.F., Ayala, I., Giandoreggio-Barranco, K., Schanda, P., (2019). Microsecond protein dynamics from combined Bloch-McConnell and near-rotary-resonance R1? Relaxation-Dispersion MAS NMR. *ChemPhysChem* **20** (2), 276–284.
44. Tollinger, M., Sivertsen, A.C., Meier, B.H., Ernst, M., Schanda, P., (2012). Site-resolved measurement of microsecond-to-millisecond conformational-exchange processes in proteins by solid-state NMR spectroscopy. *J. Am. Chem. Soc.* **134** (36), 14800–14807.
45. Igumenova, T.I., McDermott, A.E., Zilm, K.W., Martin, R. W., Paulson, E.K., Wand, a.J., (2004). Assignments of carbon NMR resonances for microcrystalline ubiquitin. *J. Am. Chem. Soc.* **126** (21), 6720–6727.
46. Huang, K.-Y., Amodeo, G.A., Tong, L., McDermott, A., (2011). The structure of human ubiquitin in 2-methyl-2,4-pentanediol: a new conformational switch. *Prot. Sci.* **20** (3), 630–639.

47. Xue, K., Sarkar, R., Tosner, Z., Lalli, D., Motz, C., Koch, B., Pintacuda, G., Reif, B., (2019). MAS dependent sensitivity of different isotopomers in selectively methyl protonated protein samples in solid state NMR. *J. Biomol. NMR* **73**, 625–631.
48. Kurauskas, V., Crublet, E., Macek, P., Kerfah, R., Gauto, D.F., Boisbouvier, J., Schanda, P., (2016). Sensitive proton-detected solid-state NMR spectroscopy of large proteins with selective CH_3 labelling: application to the 50S ribosome subunit. *Chem. Commun.* **52**, 9558–9561.
49. Bennett, A.E., Rienstra, C.M., Griffiths, J.M., Zhen, W., Lansbury, P.T., Griffin, R.G., (1998). Homonuclear radio frequency-driven recoupling in rotating solids. *J. Chem. Phys.* **108** (22), 9463–9479.
50. Smith, A.A., Ernst, M., Meier, B.H., (2018). Optimized "detectors" for dynamics analysis in solid-state NMR. *J. Chem. Phys.* **148** (4)
51. Lewandowski, J.R., (2013). Advances in solid-state relaxation methodology for probing site-specific protein dynamics. *Acc. Chem. Res.* **46** (9), 2018–2027.
52. Schanda, P., Ernst, M., (2016). Studying dynamics by magic-angle spinning solid-state NMR spectroscopy: principles and applications to biomolecules. *Prog. Nucl. Magn. Reson. Spectrosc.* **96**, 1–46.
53. Smith, A.A., Ernst, M., Meier, B.H., (2017). Because the light is better here: correlation-time analysis by NMR spectroscopy. *Angew. Chem. Int. Ed.* **56** (44), 13590–13595.
54. Napoli, F., Becker, L.M., Schanda, P., (2023). Protein dynamics detected by magic-angle spinning relaxation dispersion NMR. *Curr. Opin. Struct. Biol.* **82**, 102660.
55. Ma, P., Haller, J.D., Zajakala, J., Macek, P., Sivertsen, A. C., Willbold, D., Boisbouvier, J., Schanda, P., (2014). Probing transient conformational states of proteins by solid-state R1? Relaxation-dispersion NMR spectroscopy. *Angew. Chem. Int. Ed.* **53** (17), 4312–4317.
56. Roche, J., Girard, E., Mas, C., Madern, D., (2019). The archaeal ldh-like malate dehydrogenase from ignicoccus islandicus displays dual substrate recognition, hidden allostery and a non-canonical tetrameric oligomeric organization. *J. Struct. Biol.* **208** (1), 7–17.
57. Brochier-Armanet, C., Madern, D., (2021). Phylogenetics and biochemistry elucidate the evolutionary link between l-malate and l-lactate dehydrogenases and disclose an intermediate group of sequences with mix functional properties. *Biochimie* **191**, 140–153.
58. Urbanek, A., Morató, A., Allemand, F., Delaforge, E., Fournet, A., Popovic, M., Delbecq, S., Sibille, N., Bernadó, P., (2018). A general strategy to access structural information at atomic resolution in polyglutamine homorepeats. *Angew. Chem. Int. Ed.* **130** (14), 3660–3663.
59. K. Xue, M. Mühlbauer, S. Mamone, R. Sarkar, B. Reif, Accurate Determination of ^{1}H-^{15}N Dipolar Couplings using inaccurate settings of the Magic Angle in Solid State NMR, Angew. Chem. Int. Ed.
60. B.P. Tatman, V. Sridharan, M. Uttarkabat, C.P. Jaroniec, M. Ernst, P. Rovó, P. Schanda, Bumps on the road: the way to clean relaxation dispersion magic-angle spinning NMR, J. Am. Chem. Soc. in press. doi:10.1021/jacs.5c09057.
61. Helmus, J.J., Jaroniec, C.P., (2013). Nmrglue: an open source Python package for the analysis of multidimensional NMR data. *J. Biomol. NMR* **55** (4), 355–367.
62. Virtanen, P., Gommers, R., Oliphant, T.E., Haberland, M., Reddy, T., Cournapeau, D., Burovski, E., Peterson, P., Weckesser, W., Bright, J., van der Walt, S.J., Brett, M., Wilson, J., Millman, K.J., Mayorov, N., Nelson, A.R.J., Jones, E., Kern, R., Larson, E., Carey, C.J., Polat, İ., Feng, Y., Moore, E.W., VanderPlas, J., Laxalde, D., Perktold, J., Cimrman, R., Henriksen, I., Quintero, E.A., Harris, C.R., Archibald, A.M., Ribeiro, A.H., Pedregosa, F., van Mulbregt, P., (2020). SciPy 1.0 Contributors, SciPy 1.0: fundamental algorithms for scientific computing in python. *Nat. Methods* **17**, 261–272.
63. Hunter, J.D., (2007). Matplotlib: A 2D graphics environment. *Comput. Sci. Eng.* **9** (3), 90–95.
64. Motulsky, H., Christopoulos, A., (2004). Fitting Models to Biological Data Using Linear and Nonlinear Regression: A practical guide to curve fitting. Oxford University Press.
65. B.P. Tatman, The development of methods to study structure and dynamics in biological systems using solid-state NMR, Phd thesis, University of Warwick, available at https://wrap.warwick.ac.uk/id/eprint/185489/ (July 2023).
66. Smith, A.A., Ernst, M., Meier, B.H., Ferrage, F., (2019). Reducing bias in the analysis of solution-state NMR data with dynamics detectors. *J. Chem. Phys.* **151** (3), 034102. https://doi.org/10.1063/1.5111081.
67. Smith, S., Levante, T., Meier, B., Ernst, R., (1994). Computer simulations in magnetic resonance. An object-oriented programming approach. *J. Magn. Reson.* **106**, 75–105.
68. Ye, C., Fu, R., Hu, J., Hou, L., Ding, S., (1993). Carbon-13 chemical shift anisotropies of solid amino acids. *Magn. Reson. Chem.* **31** (8), 699–704.
69. Schanda, P., Meier, B.H., Ernst, M., (2011). Accurate measurement of one-bond H-X heteronuclear dipolar couplings in MAS solid-state NMR. *J. Magn. Reson.* **210** (2), 246–259.